Effects of Periodic Wake Passing Upon Bypass Transition of Blade Boundary Layer and Unsteady Loss

Eitaro KOYABU[1,] Ken-ichi FUNAZAKI[2] and Manabu KIMURA[3]

[1] Department of Mechanical Engineering
Sophia University

7-1, Kioi-cho, Chiyoda-ku, Tokyo 102-8554, JAPAN
Phone: +81-3-3238-3606, FAX: +81-3-3238-3606, E-mail: e-koyabu@me.sophia.ac.jp
[2] Iwate University, [3] Sony Shiroishi Semiconductor Inc.

ABSTRACT

This study investigates wake-induced boundary layer development and transition process on a flat plate, which is subjected to favorable, and adverse pressure gradients. Boundary layer loss generated by the wake passing is then quantitatively examined through detailed boundary layer measurements by use of a single hot-wire probe. The main focus of this paper is how the wake passage affects the transitional behavior of the boundary layer under the influence of favorable and adverse pressure gradients, with turbulence grid. The flow accelerating and decelerating devices are simulated the pressure gradients on the surface of the turbine blade. A spoked-wheel-type wake generator is used to simulate the unsteady flow field over the suction or pressure surface of a turbine rotor by changing the direction of the rotation of the wake-generator. Detailed boundary layer measurements are performed by use of a hot-wire anemometry, which yields analysis of raw signal of the velocity or time-averaged momentum thickness or time-averaged local loss coefficient of the boundary layer. Analysis of raw signal of the velocity is also employed in order to extract the periodic events associated with the wake passage from the acquired data. Noticeable differences in transitional behavior of the wake-affected boundary layer appear between these two wake-generating conditions. The previously observed dependence of wake-induced transition on the movement of the wake-generating bar is confirmed. It is also found that the wake passage increases the boundary layer loss.

NOMENCLATURE

d	: diameter of the wake-generating bar
D	: diameter of the turbulence grid wire
L	: length of the test model
n	: rotation per minute
n_b	: number of wake-generating bars
Re_{in}	: Reynolds number based on the length of the test model and the inlet velocity
S	: Strouhal number
t	: time
T	: wake-passing period
$\tilde{T}u$	: ensemble-averaged turbulence intensity
U_{in}	: inlet velocity
U_{local}	: local free-stream velocity
u_k	: sampled velocity data
$\tilde{u}$	: ensemble-averaged velocity
x	: surface length from the leading edge
y	: distance normal to the surface of the test model
$\tilde{\delta}$	: ensembled-averaged boundary layer thickness
$\tilde{\delta_1}$	: ensembled-averaged displacement thickness
$\tilde{\delta_2}$	: ensembled-averaged momentum thickness
$\tilde{\delta_3}$	: ensembled-averaged energy dissipation thickness

Subscripts

$^{-}$	: time-averaged value
$\sim$	: ensemble-averaged value

INTRODUCTION

It is well known that there are two types of boundary layer transition without separation. One is bypass transition, and the other is natural transition. In bypass transition, turbulent spots are directly produced in the boundary layer as a result of high free-stream turbulence. The initial phase of two-dimensional instability is bypassed in this case. Natural transition is, on the other hand, a classical process starts from the appearance of two-dimensional Tollmien-Schlichting instability waves in a laminar boundary layer.

Boundary layers on blades in turbomachines are characterized by periodical disturbances such as incoming wakes. A number of studies have therefore been made on wake-boundary layer interaction, in other words, wake-induced bypass transition of blade boundary layer far (for example, Mayle, 1991; Walker, 1993; Funazaki, 1996a, b; Funazaki, 1997; Solomon, 1996; Halsted et al., 1997a, b). However, the effect of wake passing upon this bypass transition is not fully understood yet. The transitional behavior becomes much more complicated with the existence of free-stream turbulence.

In the present study, the experimental study was performed on the bypass transition of the boundary layer on the test model subjected to periodic wake passing. The unsteady velocity field was measured with hot-wire anemometry in a simple test facility. A duct-contouring device was adopted to adjust the pressure gradient so that the same situation as in the previous work was reproduced (Funazaki (1996a,b), Funazaki and Koyabu (1999)). A spoked-wheel type wake generator was used. Measurement was done for favorable and adverse pressure gradients with free-stream turbulence intensity. Detailed hot-wire measurements were executed to obtain steady and wake-affected velocity field in the boundary layer.

EXPERIMENTAL SETUP

Figure 1 shows a schematic layout of the test facility used in this study. The settling chamber and the contraction nozzle reduced free-stream turbulence from the blower down to about 0.5%. Incoming wakes were produced by a spoken-wheel type generator that consisted of a disk with 400 mm diameter and cylindrical bars of 5 mm or 3mm diameter. Revolution number of the disk in the wake generator was counted by an optical tachometer. The fluctuation in revolution was found to be less than 0.5%. The wake generator was set so that each of the wake generating bars became parallel with the leading edge of the test model when it moved in front of the model. Figure 2 shows the test model and passage-contouring devices attached on the top and bottom walls of the test duct, which was used to generate a specified pressure gradient over the test model surface. Also shown is the system for the boundary layer measurement. The test model made of acrylic resin was 1.0 m length and had a semi-elliptic leading edge with the long axis of 75 mm and the short axis of 15 mm, followed by a flat-plate after body. The width and thickness were 200 mm and 30 mm, respectively. Static pressure taps were provided on one side of the test model to measure the pressure gradients imposed on the test surface. The flow accelerating-d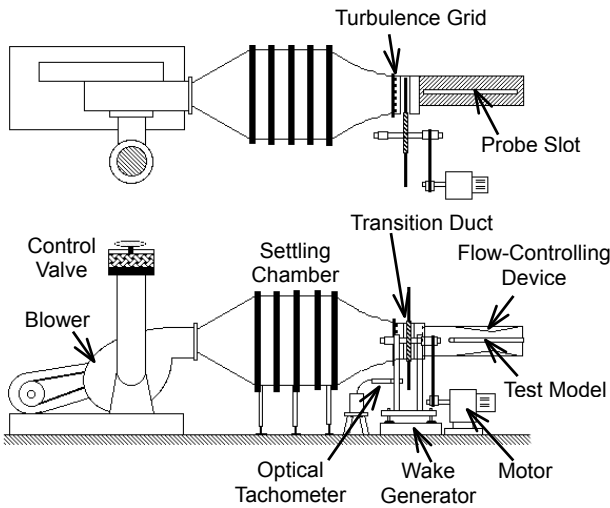ecelerating device was designed so as to reproduce the pressure gradients similar to that on the suction surface of an actual turbine blade. The flow accelerating-decelerating device had a slot along its centerline through which a hot-wire probe could be inserted into the main flow. Rotation direction of the disk of the wake generator was easily reversed, which changed the movement of the wake-generating bars relative to the model, as designated normal rotation or reverse rotation in Fig.2. Free-stream turbulence intensity was controlled using passive type grid.

INSTRUMENTATION AND DATA PROCESSING

Ensemble-Averaged Quantities. A single hot-wire probe was used to measure the boundary layer on the test model. A PC-controlled traversing unit placed the probe to the location to be measured with the precision of 0.01 mm. The probe was connected to a constant-temperature anemometer. By monitoring the free-stream temperature at exit of the test section, the temperature unit effectively compensated the temperature fluctuation of relatively low frequency during the long-running measurement. An A/D converter acquired and digitized linearized signal from the probe using once-per-revolution signal from the optical tachometer as synchronization signal, which guaranteed the application of the phase-locked averaging technique to the sampled data. The data-sampling rate was 50kHz and each of the digitized records contained 2500 words. Phase-locked or ensembled-averaged velocity, $\tilde{u}$, was then calculated from the acquired instantaneous velocity data, $u_k (k = 1,2,...,100)$ as follows:

$$\tilde{u}(x,y,t) = \frac{1}{N}\sum_{k=1}^{N} u_k(x,y,t) \qquad (1)$$

Ensembled-averaged turbulence intensity was also defined by

$$\tilde{T}u(x,y,t) = \frac{1}{U_e(x)}\sqrt{\frac{1}{n-1}\sum_{k=1}^{N}(u_k(x,y,t) - \tilde{u}(x,y,t))^2} \qquad (2)$$

where U_e was the local velocity determined from the static pressure measurements with the Bernoulli's equation. From the ensembled-averaged velocity, boundary layer integral characteristics such as displacement thickness were calculated using the following equations:
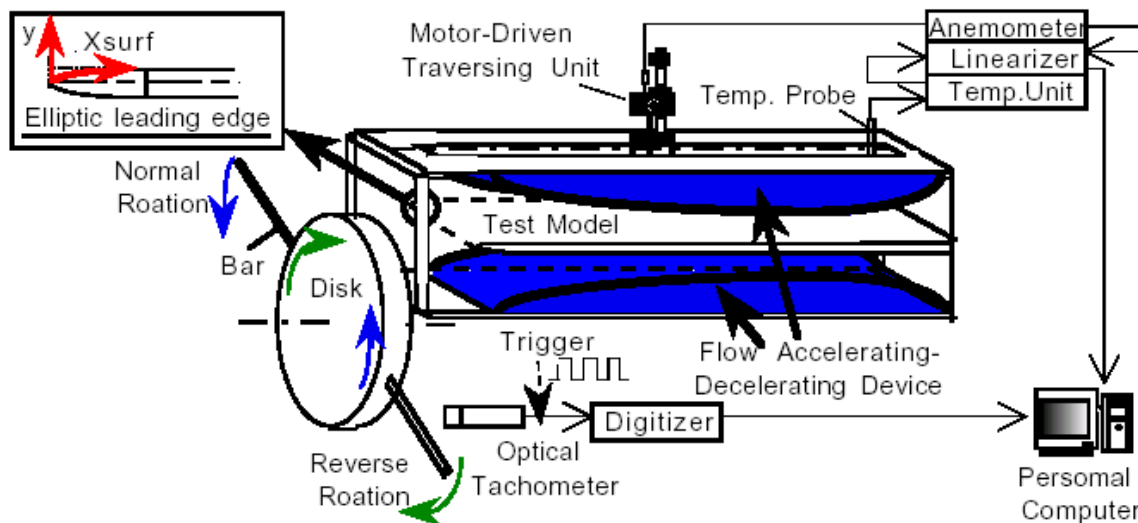

Fig.1 Test facility

Fig.2 Test model and the system for the boundary layer measurement, with an explanatory illustration of wakes generated in the normal and reverse rotation

$$\tilde{\delta}_1(x,t) = \int_0^{\delta(x,t)} \left(1 - \frac{\tilde{u}(x,y,t)}{U_e(x)}\right) dy \qquad (3)$$

$$\tilde{\delta}_2(x,t) = \int_0^{\delta(x,t)} \left(1 - \frac{\tilde{u}(x,y,t)}{U_e(x)}\right) \frac{\tilde{u}(x,y,t)}{U_e(x)} dy \qquad (4)$$

$$\tilde{\delta}_3(x,t) = \int_0^{\delta(x,t)} \left(1 - \left(\frac{\tilde{u}(x,y,t)}{U_e(x)}\right)^2\right) \frac{\tilde{u}(x,y,t)}{U_e(x)} dy \qquad (5)$$

$\tilde{\delta}$ was an ensembled-averaged boundary layer thickness, which was the distance where the ensembled-averaged velocity reached the maximum among the data acquired at the same streamwise location. Shape factor was accordingly calculated by

$$\tilde{H}_{12}(x,t) = \tilde{\delta}_1 / \tilde{\delta}_2 \qquad (6)$$

Time-Averaged Quantities.　　Time-averaged quantities were defined by the integration of the ensembled-averaged quantities over the wake-passing period as follows:

$$\overline{Tu}(x,y) = \frac{1}{T} \int_{t_0}^{t_0+T} \tilde{Tu}(x,y) dt \qquad (7)$$

$$\overline{\delta}_i(x) = \frac{1}{T} \int_{t_0}^{t_0+T} \tilde{\delta}_i(x,t) dt \qquad (i=1,2,3) \qquad (8)$$

$$\overline{H}_{12}(x) = \frac{1}{T} \int_{t_0}^{t_0+T} \tilde{H}_{12}(x,t) dt \qquad (9)$$

Intermittency factor.　To understand transitional process of the wake-affected boundary layer in detail, raw signals of the velocity are used. Time-averaged intermittency factor $\overline{\gamma}$, turbulence detector function $D(t)$ and threshold level T_r are defined by the following equations:

$$I(t) = \begin{cases} 1 & \text{when} & D(t) \geq T_r \\ 0 & \text{when} & D(t) < T_r \end{cases} \qquad (10)$$

$$D(t) = \left| \frac{\partial u}{\partial t} \right| \qquad (11)$$

$$T_r = C_{tr} \times \left(U^2 / \overline{\delta}\right), C_{tr} = 0.10 \qquad (12)$$

$$\overline{\gamma} = \frac{1}{n} \sum_{i=1}^{n} I(t) \qquad (13)$$

where turbulence detector function $D(t)$ and threshold level T_r were defined by the following equation, respectively. The onset and the end of transition were determined as the locations where time-averaged intermittency factor exceeded 0.1 and 0.9, respectively, although the true positions were likely to locate slightly upstream of the determined positions because of relatively sparse measurement points in the streamwise direction.

UNCERTAINTY

Uncertainties of the inlet velocity and instantaneous velocity were estimated to be about 2% and 3% using Kline and McClintoch method. The integral characteristics given by Eqs. (3), (4), and (5) had uncertainties of about 6%, 7% and 8%, respectively. The shape factor defined by Eq. (6) accordingly contained about 10% uncertainty.

RESULTS AND DISCUSSION

Test Conditions

Table 1 shows the test conditions of this study. Test case 1 was the baseline experiment where the inlet velocity U_{in} was 10m/s and Reynolds number Re based on the length of the test model and the inlet velocity was 6.7×10^6. The flow accelerating-decelerating device in this case was set so as to achieve front-loading type pressure gradient on the test model. Test case 3 was different from Test case 1 with respect to the arrangement of the accelerating-decelerating device, which created aft-loading type pressure gradient. Test case 2 aimed at clarifying effects of periodic wake passing upon bypass transition under low free-stream turbulence of 0.5 %. In test case 3, the test model was moved downstream by 0.3 %. Test case 4 and 5 were adopted to clarify the difference of transition due to the direction of bar rotation in comparison with the test case 3, so-called negative jet effect may be identified. In the test case 6, 7 and 8, the inlet free-stream turbulence intensity was increased by 28 %. Strouhal number S characterized wake-affected unsteady flow field around the test model as follows:

$$S = \frac{fL}{U_{in}} = \frac{nn_b}{60} \frac{L}{U_{in}} \qquad (14)$$

Inlet free-stream turbulence was about 0.5%. The measurement region extended from $x/L = 0.105$ to 0.875 in the streamwise direction and from $y/L = 0.2 \times 10^{-3}$ to 0.01 on the surface of the test model.

Static Pressure Distribution

Figure 3 shows the pressure distribution over the test model. Static pressure coefficient, C_p, is calculated by

$$C_p = \frac{P_0 - p}{1/2 \rho U_{in}^2} = \left(U_e / U_{in}\right)^2 \qquad (15)$$

Also shown is the corresponding acceleration parameter defined by the following equation:

$$K = \frac{\upsilon}{U_{in}^2} \frac{dU_{in}}{dx} \qquad (16)$$

In the test case 1 and 3, the averaged acceleration parameter was about -5×10^{-7} and 4×10^{-7}, followed by the deceleration, respectively.

Table 1　Test condition

Test Case	Rotation direction	S	Tu	Flow acceleration-decelerating device
1	–	0	0.5	Type-A
2	Normal	2.15	0.5	Type-A
3	–	0	0.5	Type-B
4	Normal	2.15	0.5	Type-B
5	Reverse	2.15	0.5	Type-B
6	–	0	1.4	Type-B
7	Normal	2.15	1.4	Type-B
8	Reverse	2.15	1.4	Type-B
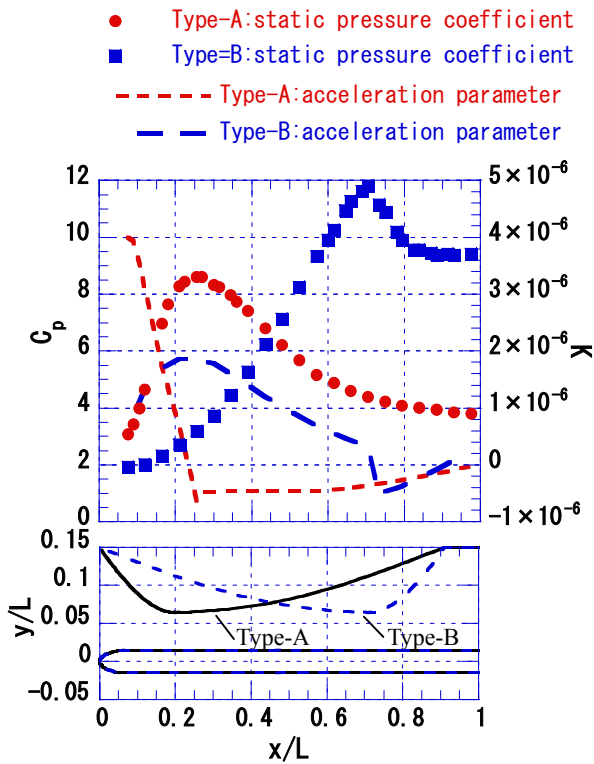
Fig.3 The pressure coefficient distribution and acceleration parameter

Fig.4 Velocity and turbulence intensity profiles in the wake generated by the wake generator (a: d=5mm, b: d=3mm)

Incoming flow condition

Figure 4 shows ensemble-averaged velocity and turbulence intensity of inside the moving wake, which were measured by the hot-wire probe located 200mm upstream of the test model during one wake passing period. The data shown here were normalized with the inlet velocity U_{in}. The velocity deficit of the wake was about 10% of U_{in}. Maximum wake turbulence intensity became about 8% for the bar diameter of 5mm, while about 5% for the bar of diameter of 3mm. With the turbulence grid, the value of the turbulence intensity between the two neighboring wake increased from 0.6% to 2.0%. But the peak values of velocity deficit and turbulence intensity don't vary substantially even under the enhanced free-stream turbulence condition.

Raw data

Figure 5 shows the raw signals of the velocity measured at $y = 0.2$ mm for 14 locations with flow accelerating-decelerating device. The data are normalized based on the local velocity U_{local}. The interval between two adjacent velocity profiles was proportional to the actual interval of the corresponding measurement locations. In test case 1 (fig.5 (a)), the amplitude of the normalized velocity data drastically changed from the leading edge to about 0.405L. Time-averaged intermittency factor is about 0.95, become turbulence transition. The test case 2 (fig.5 (b)), normalized velocity data show periodic wake passing over the test model because there are periodic velocity deficit of the wake. As the incoming wake moves away from the test model, amplitude of normalized velocity shows a wedge shape. This phenomenon promotes transition because a high turbulence in the wakes generates turbulence spots. It is observed that that the amplitude normalized velocity decreases just after the wake passage as marked by circle A. This amplitude of normalized velocity is temporarily suppressed in this region. Figure 6 also shows the raw signals of the velocity acquired at $y = 0.2$ mm for 15 locations with the flow accelerating-decelerating device type-b (case 3 and 4). From the leading edge to about 0.835% test model, the amplitude of
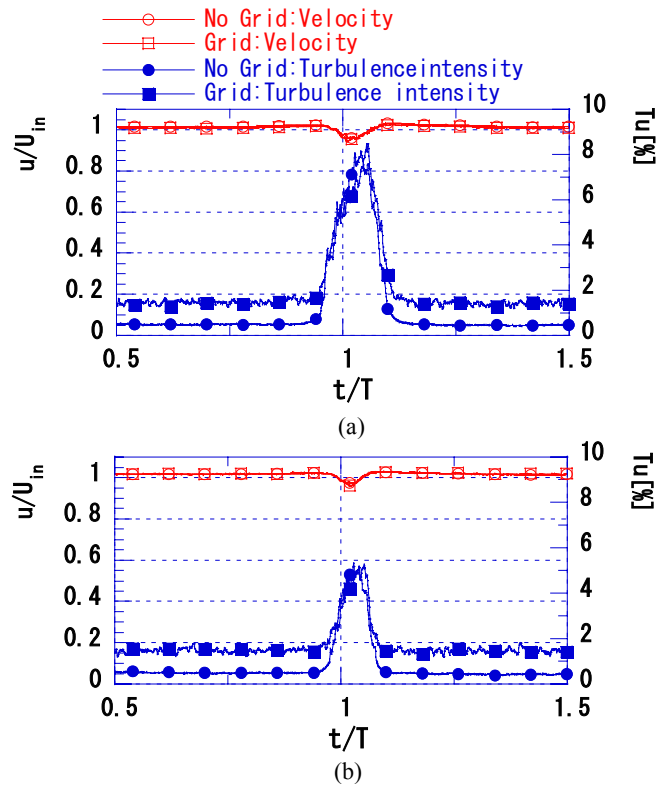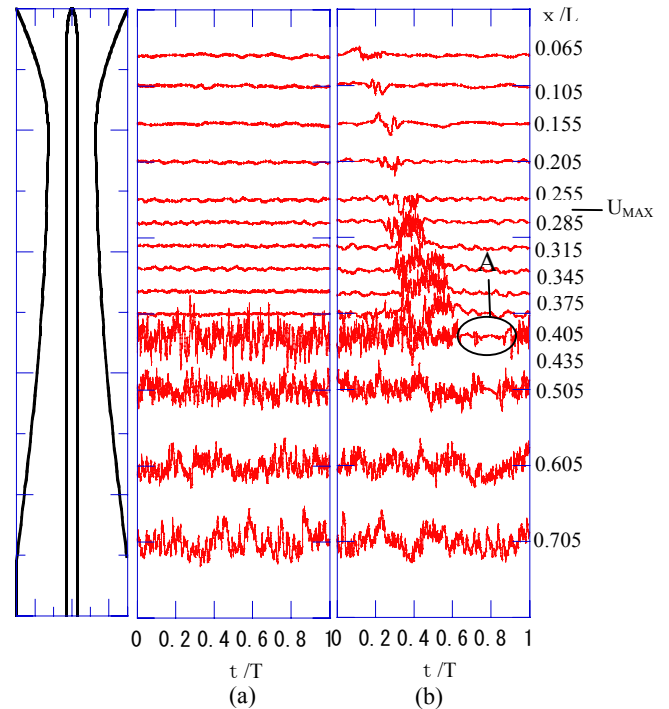

Fig.5 Raw time traces measured at y=0.2×10⁻³m for the several locations over the test model under the influence of the device type-a (a : no wake , b: normal rotation)

the normalized velocity significantly changed (fig.5 (a)). As the incoming wake moved away from the test model, amplitude of normalized velocity data shows a wedge shape (fig.5 (b)). The flow with weak acceleration led to gradual boundary layer transition in comparison with the case using flow accelerating-decelerating device type-a. The wake effect was dominant in this bypass transition in comparison with adverse pressure gradients. Likewise
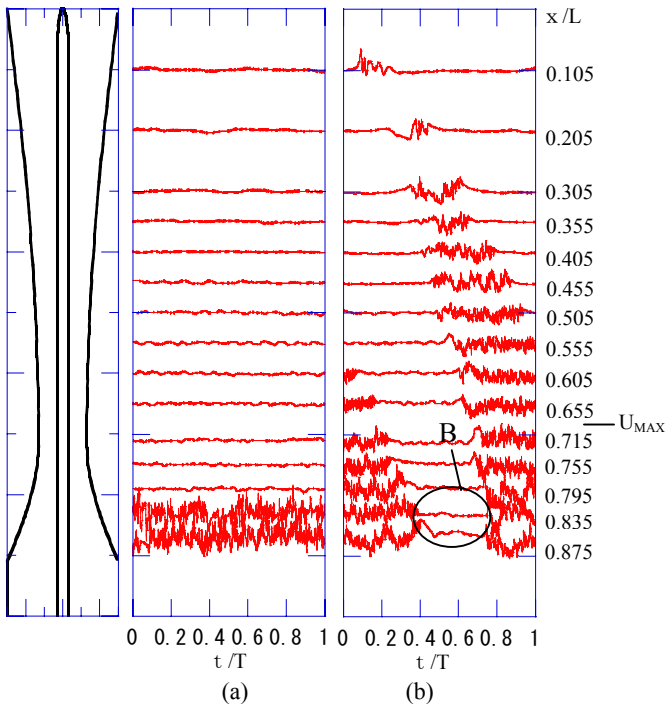
Fig.6　Raw time traces measured at y=0.2×10^{-3}m for the several locations over the test model under the influence of the device type-b (a : no wake , b : normal rotation)
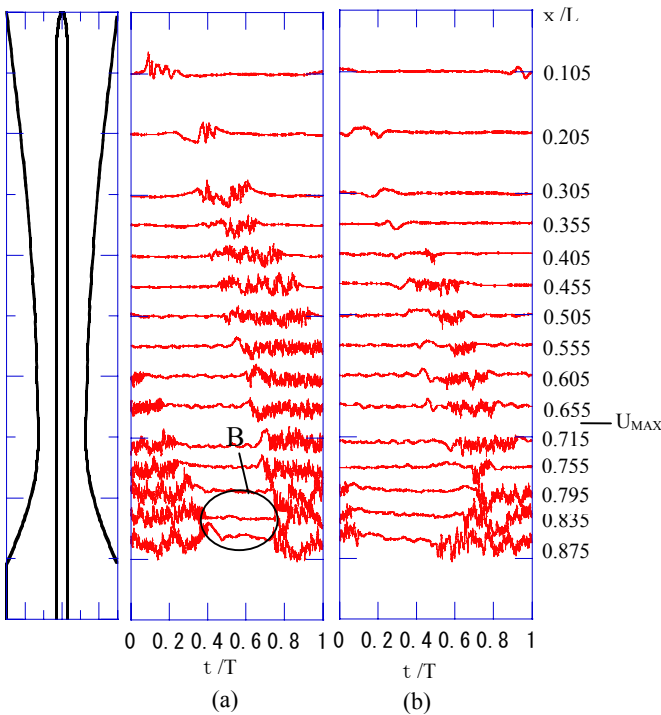

Fig.7　Raw time traces measured at y=0.2×10^{-3}m for the several locations over the test model under the influence of the device type-b (a: normal rotation, b: reverse rotation)

in test case 2, the calmed region appeared just after the wake passage as marked by circle B. Figure 7 shows the raw signals of the velocity acquired at $y = 0.2$ mm for 15 locations with flow accelerating-decelerating device type-b (case 4 and 5). The fluid inside the incoming wake relatively moved away from the test model, so that the wake width tended to become narrower than that of the normal rotation case (fig.7 (b)). Since contributions from the wake turbulence to the turbulence zone were minimal, the
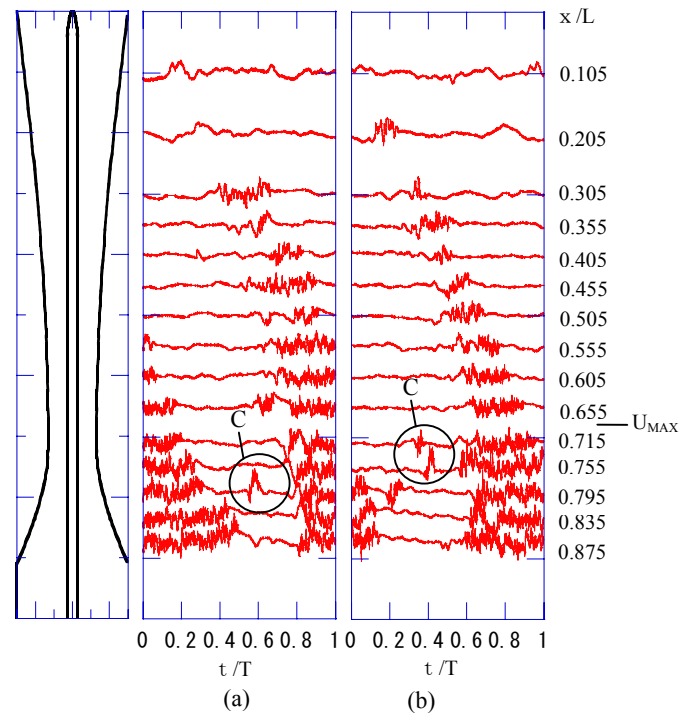

Fig.8　Raw time traces measured at y=0.2×10^{-3}m for the several locations over the test model under the influence of the device type-b with Grid (a : normal rotation, b: reverse rotation)

streamwise extent of the turbulence zone was also relatively limited. Figure 8 also shows the raw signals of the velocity acquired at $y = 0.2$ mm for 15 locations with flow accelerating-decelerating device type-b and the turbulence grid (case 7 and 8). The enhanced free-stream turbulence clearly caused localized velocity fluctuation in the velocity signal as marked by circles C (fig.8 (a), (b)). In this case, the boundary layer transition was governed by not only the wake passage but the free-stream turbulence.

Time-averaged quantity

Momentum thickness.　　Figure 9 shows time-averaged momentum thickness for test conditions. The time-averaged momentum thickness rapidly rose after the flow entered the region with the adverse pressure gradient. The flow with weak deceleration resulted in high momentum thickness. The enhanced free-stream turbulence also increased momentum thickness. It was
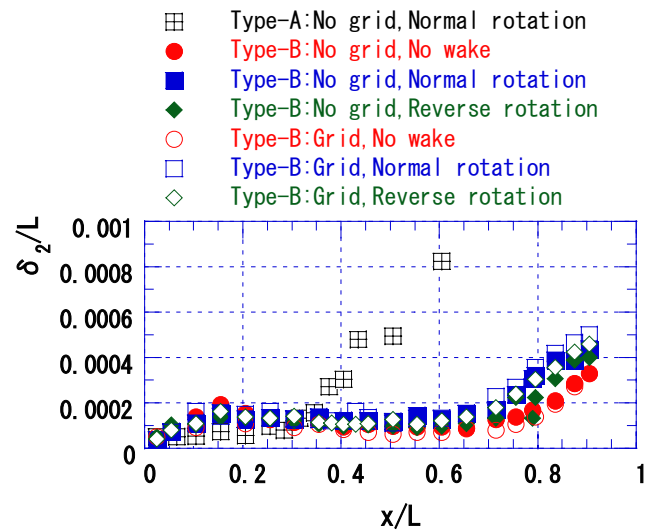

Fig.9　Time-averaged momentum thickness for test conditions

also found that there was a clear difference in the momentum between the normal and reverse rotation cases. The normal rotation case yielded higher momentum thickness than the reverse rotation case did, which could be attributed to negative-jet effect.

Local loss coefficient.   Figure 10 shows local loss coefficient under the effect of the wake passage, free-stream turbulence intensity, favorable and adverse pressure gradients. Local loss coefficient, $\Delta\zeta$ is defined by

$$\Delta\zeta = \left[\frac{U\left(x_{surf}\right)}{U_{in}}\right]^3 \frac{\delta_3}{L} \qquad (17)$$

Figure 10 (a) shows local loss coefficient with no grid. The local loss coefficient exhibited abrupt increase from the beginning of the adverse pressure gradient for both flow accelerating-decelerating devices. In the case of type-a, the wake passage did not nearly affect boundary layer bypass transition. On the other hand, in the case of type-b, there appeared noticeable effects of the periodic wake passage upon the boundary layer bypass transition. Figure 10 (b) shows local loss coefficient with turbulence grid. The free-stream turbulence played a dominant role in the bypass transition in comparison with the periodic wake passage higher

than that induced by periodic wake passage for inlet free-stream turbulence cases.

CONCLUSIONS

This study dealt with hot-wire probe measurements of boundary layer bypass transition. The focus of this study was on the effects of periodic passing wakes on the boundary layer development and the relation of the boundary layer loss. The findings in this study can be itemized as follows.

1) In the case of the flow accelerating-decelerating device type-a, the wake passage did not nearly affect boundary layer bypass transition. On the other hand, in the case of the flow accelerating-decelerating device type-b, there appeared noticeable effects of the periodic wake passage upon the boundary layer bypass transition.

2) From both flow accelerating-decelerating devices, the normal rotation case yielded higher wake width than the reverse rotation case did, which could be attributed to negative-jet effect. The calmed region, which appeared just after the wake passage, is temporarily suppressed amplitude of normalized velocity.

3) The free-stream turbulence played a dominant role in the bypass transition in comparison with the periodic wake passage higher than that induced by periodic wake passage for inlet free-stream turbulence cases.

4) The time-averaged momentum thickness and time-averaged loss coefficient exhibited abrupt increase from the beginning of the adverse pressure gradient for both flow accelerating-decelerating devices.

Fig.10   Time-averaged local loss coefficient for test conditions

REFERENCES

Halstead, D. E., et al., 1997a, "Boundary Layer Development in Axial Compressors and Turbines: Part1 of 4 - Composite Picture," *ASME Journal of Turbomachinery*, Vol.119 pp.114-127.

Halstead, D. E., et al., 1997b, "Boundary Layer Development in Axial Compressors and Turbines: Part3 of 4 – LP Turbine," *ASME Journal of Turbomachinery*, Vol.119 pp.225-237.

Funazaki, K., 1996a, "Unsteady Boundary Layers on a Flat Plate Disturbed by Periodic Wakes: Part I - Measurement of Wake-Affected Heat Transfer and Wake Induced Transition Model," *ASME Journal of Turbomachinery*, Vol.118, 327-336.

Funazaki, K., 1996b, "Unsteady Boundary Layers on a Flat Plate Disturbed by Periodic Wakes: Part II - Measurements of Unsteady Boundary Layers and Discussion," *ASME Journal of Turbomachinery*, Vol.118, pp.337-346.

Funazaki, K., Koizumi, K., Koyabu, E, 1998, "Studies on Aerodynamic Loss Due to Wake-Disturbed Boundary Layer on a Flat Plate," The Japan Society of Mechanical Engineers (B), Vol. 64, pp.2935-2941 [in Japanese].

Funazaki, K. and Koyabu, E., 1999, "Effect of Periodic Wake Passing upon Flat-Plate Boundary Layers Experiencing Favorable and Adverse Pressure Gradients," *ASME Journal of Turbomachinery*, Vol.121 pp. 333-340.

Funazaki, K., Kitazawa, T., Koizumi, K., Tanuma, T., 1997, "Studies Wake-Disturbed Boundary Layers under the Influences of Favorable Pressure Gradient and Free-stream Turbulence-Part I : Experimental Setup and Discussions on Transition Model," ASME Paper 97-GT-52.
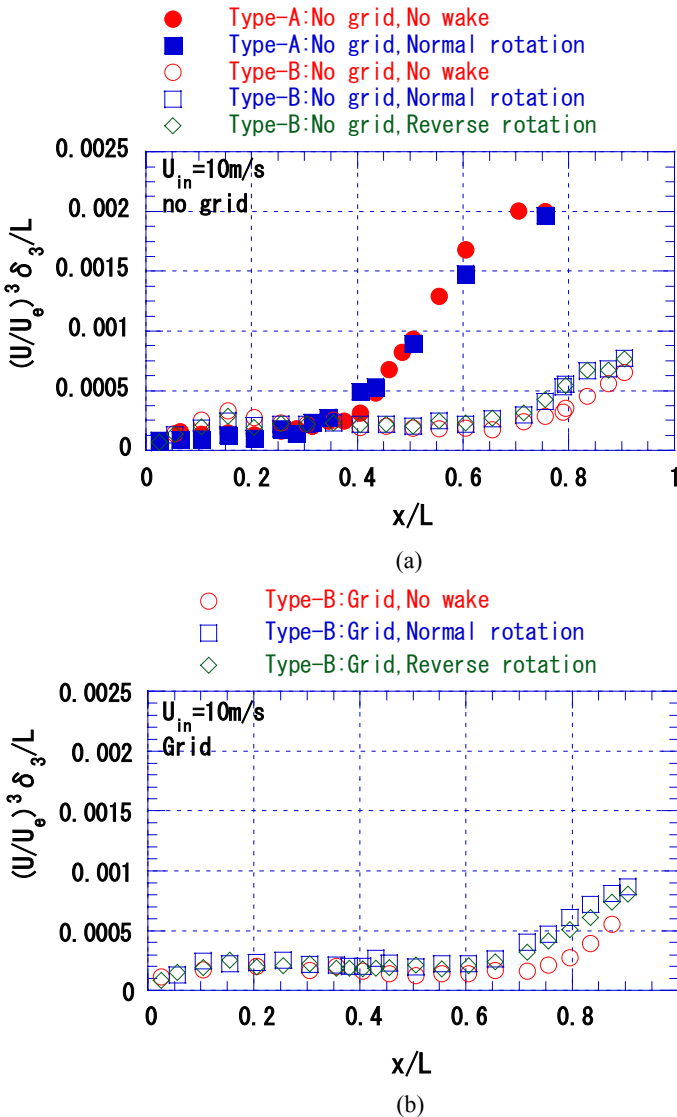
Funazaki, K., Yokota, M. and Yamawaki, S., "The effects of

Periodic Wake Passing on Film Effectiveness of Discrete Cooling Holes around the leading Edge of a Blunt Body," ASME Paper 97-GT-52.

Mayle, R. E., 1991, "The Role of Laminar-Turbulent Transition in Gas Turbine Engines," *ASME Journal of Turbomachinery*, Vol. 113, pp.509-537.

Schubauer, G. B. and Klebanoff, P. S., 1955, "Contribution on the mechanics of boundary layer transition," NACA TN 3489.

Solomon, W. J., 1996, "Unsteady boundary layer transition axial compressor blades," Ph.D. Thesis, University of Tasmania, Tasmania

Walker.G.J., 1993, "The Role of Lamina-Turbulent Transition in Gas Turbine Engines: A Discussion," *ASME Journal Turbomachinery*, Vol. 115, pp.207-217.